Origami-inspired acoustic transducer arrays: a first design and characterization study

Undergraduate Honors Thesis

Presented in Partial Fulfillment of the Requirements for Graduation with Distinction in the Department of Mechanical and Aerospace Engineering of The Ohio State University

By

Danielle Lynd

Undergraduate Program in Mechanical Engineering

The Ohio State University

May 2017

Thesis Committee:

Ryan L. Harne, Advisor

Carlos Castro

ABSTRACT

Linear or planar arrays of acoustic transducers are used to direct and focus acoustic energy through active phase delays and amplitude weights provided to the individual transducers. These acoustic transducer arrays are used in numerous important applications including medical imaging, sonar, and communications. Exiting acoustic transducer arrays are challenged in their ease of implementation and portability due to the number and spatial distribution of transducers that are required to achieve substantial acoustic energy focusing. Thus origami-inspired acoustic transducer arrays that change shape through simple mechanical folding of the array are created to provide solutions to existing beamforming obstacles. These foldable acoustic transducer arrays have several distinct advantages over the current technology, including decreased computational complexity, increased portability, and ease of implementation. This research seeks to characterize how arrays inspired by different origami tessellations and folding arrangements affect the guiding of acoustic energy. In this research, a simple, iterative computational approach is created to facilitate the design of origami-inspired acoustic transducer arrays which can direct and focus sound as desired. First, a selection of different origami tessellations are chosen as bases for new acoustic transducer arrays. These tessellations are chosen from or inspired by existing origami tessellations in literature or created through origami topology optimizers which assist in the creation of new tessellations. The tessellations are then folded in an origami simulator and visually inspected to determine if they exhibit the characteristics including compactible folding shapes, dramatic change in position of facets through folding, and lens-like curvatures. The tessellations are then evaluated in a model that utilizes a boundary element method that simulates the corresponding sound radiation properties of an acoustic transducer or transducer array fashioned according to the tessellated geometry. These results show how new origami inspired transducers and transducer arrays may significantly direct and focus acoustic waves using different degrees of folding the tessellated transducer shape.

ACKNOWLEDGEMENTS

I first want to acknowledge the generous support of the Acoustical Society of America's Robert W. Young Award for Undergraduate Research in Acoustics, which financially supported this project.

Thank you to my advisor, Dr. Ryan Harne, for all of his assistance over the course of this project. His instruction, tireless efforts, and advice on the importance of patience and persistence have been invaluable.

Thank you to Dr. Carlos Castro, for his help and support as my committee member.

Thank you to Chengzhe Zou for his support over the past year, to our intern Joseph Crump, and to all of the members of the Laboratory of Sound and Vibration Research.

TABLE OF CONTENTS

LIST OF FIGURES

LIST OF TABLES

1 Introduction

1.1 Background

The guiding of acoustic energy in real time is an important process in many engineering applications. Phased acoustic arrays are used to determine the sources of noise in jets [1] [2] and in rocket engines [3]. Acoustic arrays of source and receiver transducers that require focused sound are used in biomedical ultrasonic imaging [4] [5]. Lithotripsy is a process of destroying kidney stones that uses focused sound waves to target and fragment the kidney stones [6]. Ultrasonic therapy is also used to treat cancer by locally heating the locations where tumors exist, via focusing acoustic waves [7].

Given this interest in guiding acoustic energy, techniques have arisen that allow for the real-time guiding of acoustic energy. One technique, known as beamforming, is to assemble acoustic transducers into arrays in order to create a desired sound field [8]. Phase delays between the activation of the transducers and amplitude weights among the transducers are utilized in order to artificially create constructive and destructive interference, allowing for acoustic beams to be directed or focused [5]. Yet, such digital control of the acoustic wave fields come with a set of unique challenges. Arrays that require better focused or more directive sound energy must employ many transducers distributed over large spaces, creating a computational burden for real-time control, limiting portability, and increasing complexity of implementation [9] [10]. These problems motivate the exploration of unconventional methods of shaping and focusing acoustic energy. The use of origami-inspired acoustic transducer arrays has been examined as a way to bypass these challenges [11].

Origami has served as an inspiration for innovation in the fields of architecture and engineering. The mechanical properties of an origami fold can be tuned through small adjustments to the crease patterns of the fold [12] [13]. They can also be used to design flat-foldable, deployable structures, which fold to smaller shapes for portability [14]. Origami patterns are built on periodic patterns of planar facets, and this research team leverages the similarities between these planar surfaces and the planar surfaces of acoustic transducers in order to propose a new idea: that of a foldable acoustic transducer arrays [11]. Harne and Lynd [11] have previously explored development of such arrays.

1.2 Previous research efforts

Harne et al [11] has observed that the planar acoustic transducers may be bonded to the planar facets of origami, creating an acoustic transducer array that folds like the origami tessellation [11]. The position of the transducers is easily adjusted through simple folding, and these dramatic changes in topology can greatly influence the pattern of acoustic energy produced by the array [11]. Thus, this team leaves behind the active phase delays of the existing technology to instead focus on folding-induced changes in topology to guide acoustic energy. All transducers are kept in phase and are driven or sensed in parallel, greatly simplifying implementation of the arrays. Finally, origami-inspired patterns may be folded into compacted shapes for ease of portability. In these ways, the new technology of a foldable acoustic transducer array

bypasses the challenges of the existing acoustic transducer array. Initial research by this team concentrated on the development of an array inspired by the Miura-ori fold [11] [15].

Miura-ori was chosen as a subject for study as it is an extensively studied origami folding pattern that has several unique properties which make it useful as a substrate for a foldable transducer array. For instance, the Miura-ori tessellation is flat-foldable, so such an array may be compacted for ease of transport. It has single degree-of-freedom motion that allows the positions of transducers which are bonded to the facets of the origami pattern to be rearranged simply easily through the folding motions of the origami tessellation. [16]. The acoustic properties of a Miura-ori-inspired acoustic transducer array were determined through the use of computer simulation and experimentation which validated the model.

Miura-ori-inspired acoustic transducer arrays were shown to greatly influence the radiation of acoustic energy through simple, folding-induced topological changes. Yet, Miura-ori is limited in its folding capabilities; unlike many other origami folding patterns, it is a planar folding pattern that undergoes only 2-dimensional deformations. The next step to this research is to explore the capabilities of different origami folds in order to characterize how different tessellations may direct or focus energy in unique ways. Yet due to the breadth of origami tessellations available in literature, let alone the additional number that may be derived or newly created, an ordered process is necessary to guide efforts to design and evaluate new origami tessellations as bases for foldable acoustic transducer arrays.

1.3 Research goal

The goal of this research is to characterize the influences of different tessellations and folding arrangements on the sound radiation characteristics of such an origami-inspired acoustic transducer or transducer array. To aid in this exploration, a streamlined, iterative design process is created which allows for the efficient design and evaluation of new transducer arrays. This work seeks to examine this process by creating and evaluating several new tessellations to see how they direct and focus energy.

1.4 Overview of thesis

This thesis describes a set of integrated procedures to design new tessellations to be used as foldable, adaptive acoustic transducers and arrays based on a series of computational modeling techniques. Section 2.1 overviews the experimental methods used to develop or design a new origami folding pattern. Section 2.2 outlines the use of computer simulations that create a mesh of the folded state of the origami tessellation for evaluation in boundary element method (BEM) computations. BEM simulates the acoustic behavior of the design. Section 3 outlines four origami tessellations created using this process and provides an overview of the results of BEM analysis, as well as discusses their significance. Section 4 summarizes the conclusions made in this work and provides recommendations for future works.

2 Design Process

As established in this research, there are three primary steps in the development and evaluation of a new tessellation to be considered as a foldable acoustic transducer or transducer array, depicted by the flowchart in Figure 1. The first step is the development of a new tessellation, through topology optimizers or through inspiration from existing literature. The second step uses computer simulation to fold the tessellation. The final step evaluates the acoustic properties of the tessellation by utilizing the Boundary Element Method to simulate the sound pressure level at at points in space around the center of the array. These steps are explained further in the following sections.

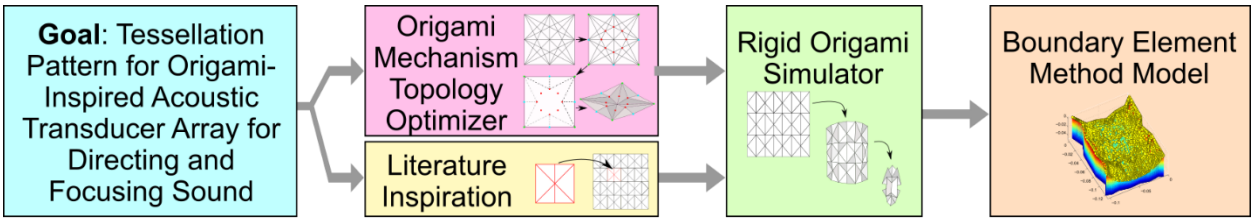

Figure 1: There are three steps in the creation of a new origami tessellation and the evaluation of its effectiveness as a substrate for an acoustic transducer array. First, an origami tessellation is designed either through the use of an origami topology optimizer or by taking inspiration from literature. The tessellation is then folded in the Rigid Origami Simulator and the coordinates of the folded states imported into a Matlab model to make a mesh. A model that uses the Boundary Element Method uses the mesh to simulate how sound emitted by the array radiates in space.

2.1 Designing a new origami tessellation

Central to the creation of new acoustic transducer arrays is the design of new origami folding patterns upon which the array can be based. In this research, there are several characteristics that a tessellation must display to be most useful.

To maintain ease of assembly, it is important that (i) the folding pattern of the substrate be created from simple mountain and valley folds on a single sheet of plastic. A tessellation must also (ii) be foldable to an extent that increases its portability, where flat-foldability, which is a full elimination of volume, is considered as the most portable of an origami tessellation. The origami folding pattern should (iii) display large topological change through folding, as these folding-induced changes are what affect changes in the guiding of acoustic energy. Finally, it is advantageous to produce a design that (iv) demonstrates signs of lensing as characterized by the development of satellite-like shapes through folding, as these curved shapes may produce a focal point at which there is greater sound energy focusing. These four design characteristics are referenced in the design of new tessellations to determine if these new folding patterns exhibit the ideal characteristics of a foldable transducer array. In the following sections, we characterize two approaches to designing new origami tessellations.

2.1.1 Literature-inspired tessellation

The first approach in creating a new origami folding pattern is to take inspiration from literature. There are a wide variety of existing origami tessellations in academic literature that can be explored in the selection

of a new acoustic transducer array design. Evans [14] characterizes several rigidly foldable tessellations, including the Yoshimura pattern, Miura-ori, and Baretto's "Mars." Sareh and Guest [17] [18] have characterized isomorphic and non-isomorphic adjustments to Miura-ori. In these papers, they have shown that adjustments to the commonly studied Miura-ori pattern can be used to create new, flat-foldable origami tessellations that are globally planar or globally curved [17] [18]. Both planar and curved origami patterns provide unique opportunities for directing or focusing acoustic energy.

In our research, we adopt the techniques of Sareh and Guest [17] [18] of adjusting existing folding patterns to develop new ones that display desired characteristics. A baseline folding pattern such as Miura-ori is created in a software application that accommodates vector images (SVG, scalable vector graphics), like Inkscape or Adobe InDesign, where the positions of lines and nodes can be manipulated easily.

One folding pattern adapted from literature is the waterbomb array, which is shown in Figure 2. Red lines indicate valley folds, while blue lines represent mountain folds. The waterbomb unit cell, shown in Figure 2(a) is a common constituent other origami tessellations. In part of this work, it is modified into the design shown in Figure 2(b). This allows it to be assembled into the array in Figure 2(c), where the top and bottom rows are shifted by half a cell away from the middle row. Figure 2(d,e) depict two of the folded configurations of this tessellation. The inward, cylindrical folded shape may introduce a focal point where near field focusing may occur so this tessellation will be considered in the following acoustic assessments.

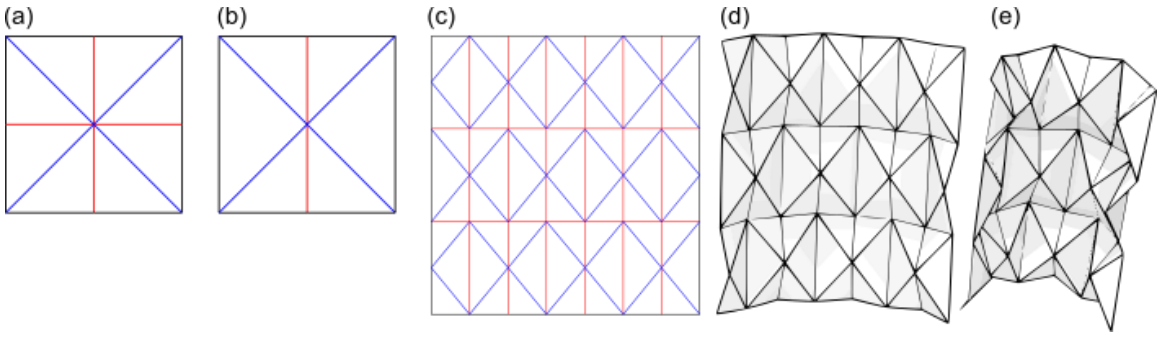

Figure 2: The waterbomb unit cell in (a) is modified slightly to its form in (b), in order to enable the assembly of the array in (c). The cells in the top and bottom rows of the array are shifted by half a cell with reference to the middle row. Two folding arrangements are depicted in a (d) slightly folded configuration to (e) more folded configuration. This tessellation forms a cylindrical shape as it is more folded which may be advantageous for near field focusing.

Both the single waterbomb constituent in Figure 2(a) and the array depicted in Figure 2(c,d,e) display three-dimensional folding shapes that may introduce focusing. Both the waterbomb unit cell and the array will be explored in Sections 3.1 and 3.3.

2.1.2 Computer-generated origami designs

Using inspiration from literature can be a time-consuming process because one must find folding patterns that display several specific desired physical characteristics. A computer-aided process could significantly reduce the time it takes to create such a tessellation. This part of the process is in part facilitated by the use of origami topology optimizers. Topology optimizers have been studied extensively. Bendsoe and Kikuchi [19] developed a topology optimization method to solve structural problems. Optimization techniques have

since been adopted and used to develop origami topology optimizing programs. Lang [20] developed the TreeMaker software, which utilizes a nonlinear constrained optimization code. This software has been especially effective in the exploration and simulation of origami tessellations. One important application of this type of simulation is in the simulation of the folding of airbags [20] [21]. Fuchi et al. [22] have investigated the use of topology optimization in the design of origami-based mechanisms. Their methodology seeks to create a way to design compliant mechanisms based in origami by creating an optimization problem of distributing fold and facet stiffness.

In this work, the Origami Mechanism Topology Optimizer (OMTO) software is utilized to facilitate the design of new origami folding patterns that demonstrate desired characteristics, including origami mechanisms [22]. Based on several input conditions described in detail in the following paragraph, the software generates a pattern of mountain and valley folds that satisfy the input conditions. OMTO was chosen as the best software for use in this process for several reasons. First, the folding pattern OMTO generates exists on a single sheet and consists of only mountain and valley folds, allowing for ease of assembly. Second, OMTO allows the placement of input conditions in three dimensions, which is useful in designing origami with out-of-plane folding behaviors. On the other hand, OMTO does not allow a condition that will specify flat-foldability, so folding patterns must be tested manually to determine if this condition is met. Some small adjustments may need to be made to a generated tessellation to ensure that the folding pattern may be folded enough to be portable. Yet, this software is a valuable tool in the design of new origami tessellations and the following steps outlined in this paper allow the user to simply determine the acoustic behaviors of beamformers based on these tessellations.

One folding pattern created using OMTO is termed the four-pointed star. Figure 3 displays the inputs and outputs of OMTO that produce this design. At the top left is an image of the conditions that are input into OMTO. These include matched and fixed boundary conditions, input forces, and optimization points along a ground structure. Red squares represent applied forces, blue triangles represent fixed boundary conditions, cyan triangles represent matched boundary conditions, and green circles represent optimized output nodes. The program then generates fold lines along the ground structure that satisfy these input conditions. The image at the bottom right of this figure depicts the fold lines that are generated for these input conditions. The top right image shows a model of the folded tessellation. In order to make this tessellation more compactible, a slight adjustment was made to the OMTO output, which is shown in the images to the right of the graph. Two diagonal valley lines were added to the folding pattern, as indicated by the green lines in the folded configurations in Figure 3. Those two images represent the folded configurations of this new, adjusted tessellation of the four-pointed star.

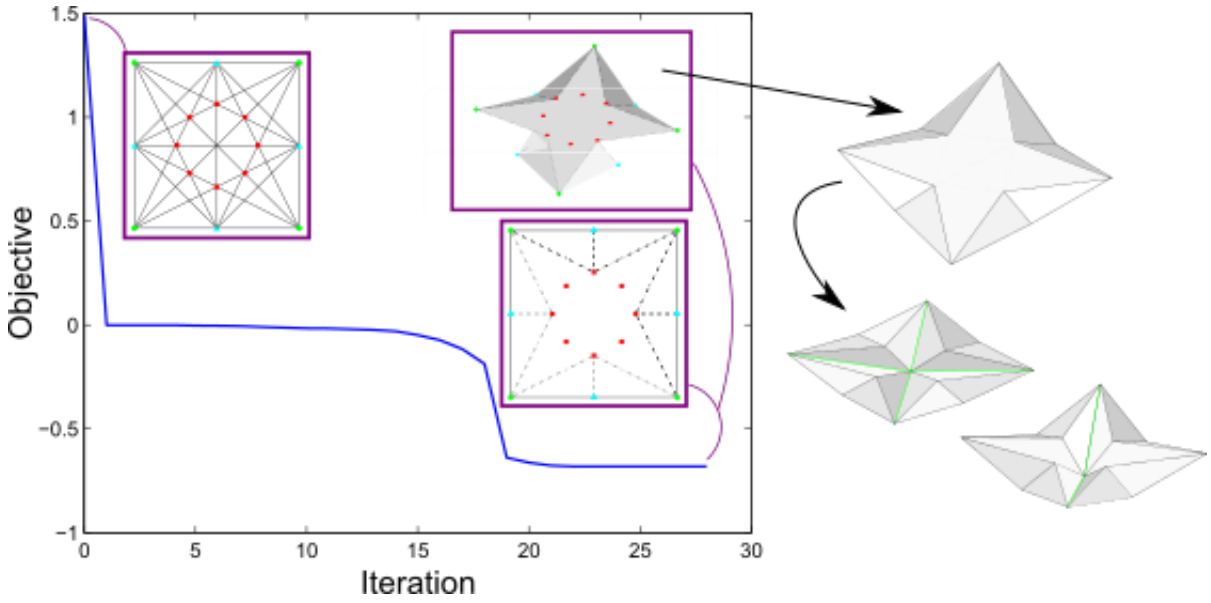

Figure 3: The figures contained in the graph on the left indicate the OMTO inputs and outputs that produce the four-pointed star tessellation. The top left image indicates the input conditions, including boundary conditions, input forces, and optimization points, that are placed on a ground structure. The images to the right represent the folding pattern produced and a model of what the tessellation may look like folded. A slight adjustment in the form of additional valley lines, as shown by the green lines in the images at the right, allows the tessellation to be compacted for greater ease of transport. The final two folded images represent two folded configurations of the final folding pattern of the four-pointed star.

The principles of this tessellation can be adopted and expanded for different tessellations. At its core, this folding pattern presents an alternating mountain and valley fold sequence that meet at the center of a square with angled outer edge features. The radial symmetry of this tessellation can be easily adapted to produce a star with more points. Figure 4(a) depicts the four-pointed star tessellation and Figure 4(b) depicts the six-pointed star tessellation, where red lines stand for mountain folds and blue lines for valley folds. Both tessellations have alternating mountain and valley folds that meet at the center and enable three-dimensional folding shapes. The outline that connects these alternating lines in both figures is a mountain fold, and its projection of a "star"-like shape are what give these tessellations their names. Blue valley folds are used to connect the outer vertices of the "star" shape to the edge of the rectangular boundary. The similarities between these tessellations are evident by comparing Figure 4(c) with the folding shapes of the four-pointed star as indicated in Figure 3. Studying the acoustical properties of the six-pointed star as compared to the four-pointed star could provide information about how very small adjustments to folding pattern may affect the radiation acoustic waves from the surfaces of these folding patterns.

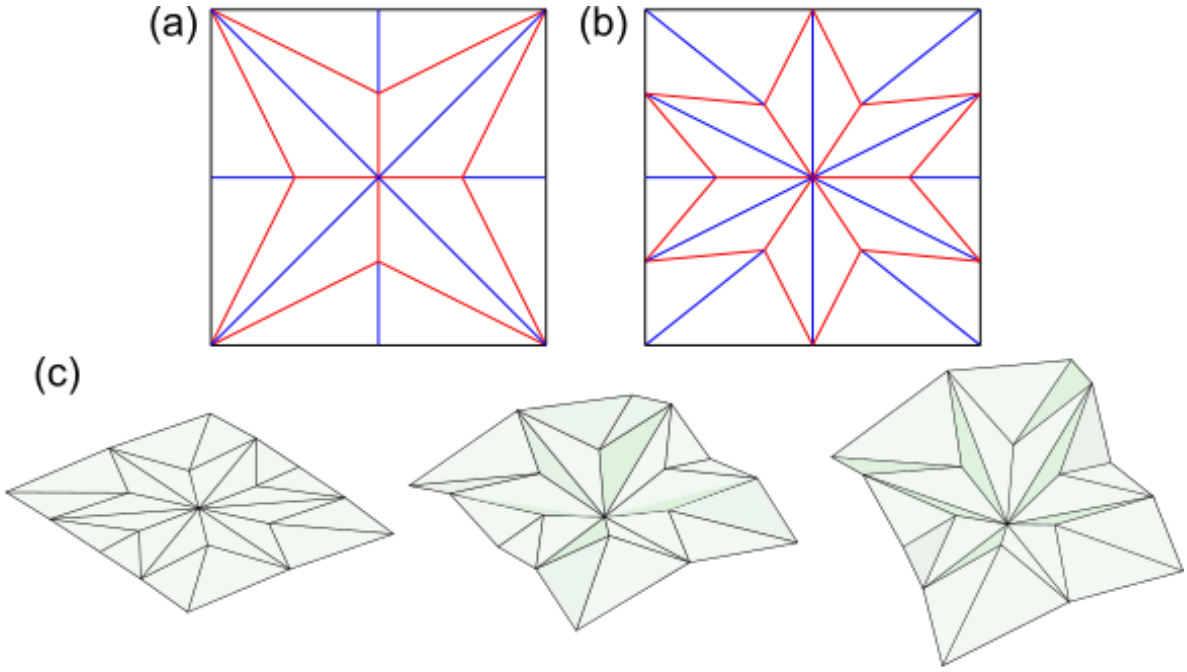

Figure 4: The tessellations of the four-pointed star (a) and the six-pointed star (b) are presented. The shared characteristics between them are most evident in the red, mountain folds that outline the "star" image, and the alternating mountain and valley folds at the center. The unfolded, slightly folded, and more folded configurations of the six-pointed star are in (c).

2.2 Rigid Origami Simulator

Once tessellations, such as the waterbomb array and the four-pointed star, are created, it is necessary to evaluate the usefulness of acoustic transducer arrays that use these tessellations as a substrate. This is done through the use of the boundary element method (BEM) to simulate acoustic wave propagation in space. However, the BEM code requires a mesh of the tessellation that is being tested in order to undertake the simulations. The coordinates of the different folding arrangements of the tessellations are required.

To identify all of the tessellation's node locations and element reconfigurations associated with the folding operations, we turn to Tomohiro Tachi's Rigid Origami Simulator (ROS) [23]. ROS utilizes a rigid origami model to simulate the folding of an origami tessellation in discrete steps [24]. The folding pattern is created in an SVG editor and imported into the ROS program. There are several benefits to using ROS. First, because the ROS generates an image of the tessellation as the folding steps are increased, researchers may visually inspect a tessellation's folding characteristics to determine if it will fit necessary requirements, such as cylindrical or spherical folding shapes. This allows for a simple and efficient iterative design process as small adjustments to folding patterns can be made relatively easily. The alternative would be to physically create the origami tessellations out of paper or plastic, which is a much more time consuming process that will result in wasted materials. Second, ROS outputs the coordinates of the vertices of the origami tessellation. These coordinates can be extracted and imported into the BEM code to reconstruct a mesh of the origami tessellation in that specific position.

2.3 Using the boundary element method to model

The boundary element method is used to find solutions to boundary integral equations [25]. For this work, it is used to solve the Helmholtz integral equation to determine the sound pressure level (SPL) that is radiated from the source. In this study, the BEM simulations are implemented in the openBEM code architecture 37 in MATLAB. All computations are conducted on a computer outfitted with an Intel Core i7-4790 processor and 32 GB of memory. The boundary element meshes are closed around the activated area of the foldable acoustic transducer or transducer array, similar to a box enclosure around a loudspeaker. Due to standard requirements for accuracy in BEM simulations, all results reported hereafter use at least 6 elements per acoustic wavelength to ensure accurate of the numerical simulations is ensured.

3 Results and Discussion

Four tessellations are produced using the process outlined in the preceding section: the adjusted waterbomb array shown in Figure 2(c), the four-pointed star tessellation in Figure 3, the waterbomb unit cell in Figure 2(a), and the six-pointed star tessellation in Figure 4. These four tessellations are studied using the BEM model to compute how they radiate sound.

There are two types of acoustic wave guiding features that are of specific interest in many applications: directivity and focusing. Directivity is the angular variation of acoustic wave radiation in the far field. A location in space is said to be in the acoustic far field when the spherical waves emitted from a source are most similar to plane waves. Focusing is defined as in increase sound pressure level emitted by a source as the radial distance increases between source and receiver. Focusing does not occur naturally, and is artificially created using technology like acoustic transducer arrays. Focusing is only a property observed in the near field.

The folding of the adjusted waterbomb array detailed in Section 3.1 suggests an opportunity both for near field focusing and for changes in directivity based on folding and frequency. The folded configurations of the four-pointed star tessellation in Section 3.2 may indicate differences in far field directivity between two folded configurations and between four different azimuth angles. Section 3.3 compares the same-sized waterbomb unit cell and six-pointed star tessellations and their ability to focus sound in the near field.

3.1 Waterbomb array

Two configurations of the waterbomb tessellation are simulated using BEM, one more folded than the other. The BEM results for a frequency of 3000 Hz are depicted in Figure 5 below. The column on the left, Figure 5(a,c,e), are the BEM results for the less folded configuration at an increasing radial distance of 0.0194 m, 0.125 m, and 0.625 m respectively. The third row, Figure 5(e,f),simulates SPL in the far field, while the first two rows, Figure 5(a,b,c,d), are evaluated in the near field. The column on the right, Figure 5(b,d,f), shows the BEM results for the more folded configuration at the same radii. The extent of folding is depicted in the inserts in each quadrant of the figure. Each of the surface plots represents the sound pressure level (SPL) in dB that is radiated from the center of the array, so that the radial distance from a point (0,0,0) in the figure and the associated color are both used to indicate the SPL at that radial location in space. The results are depicted at elevation angles from 0˚-90˚, where an elevation angle of 0˚ is along the line perpendicular to the unfolded plane of the tessellation. This elevation angle is termed as broadside.

There is a 13 dB increase in broadside SPL as the radius increases from 0.0194 m in Figure 5(a) to 0.0125 m in Figure 5(c). This significant increase in broadside SPL indicates that focusing occurs at this radial distance. Likewise, the more folded configuration sees an increase in broadside SPL between Figure 5(b) to Figure 5(d), though this increase is only around 6 dB. This again indicates the focusing abilities of this array, though it does demonstrate that folding reduces the degree to which the beam is amplified.

Folding also influences the sound radiation patterns at the same radial distance. The area of low SPL, also called a node, at the radius of 0.125 m becomes deeper from the less folded configuration in Figure 5(c) to Figure 5(d). There is also a significant SPL reduction present in Figure 5(a) which is not present at the more folded configuration of Figure 5(b).

In the far field, there is a reduction from 88 dB to 87 dB between Figure 5(c) and Figure 5(f) as the tessellation becomes more folded. Additionally, the depth of the node pictured in both Figure 5(c) and Figure 5(f) reduces through folding. At this low frequency, the acoustic wave radiation is largely uniform, so there are less clear differences between the far field radiation of the two folded configurations. In Figure 6, the same folded configurations of the waterbomb array are examined at 9 kHz. In this set of results, the influences of folding on far field radiation are more clear.

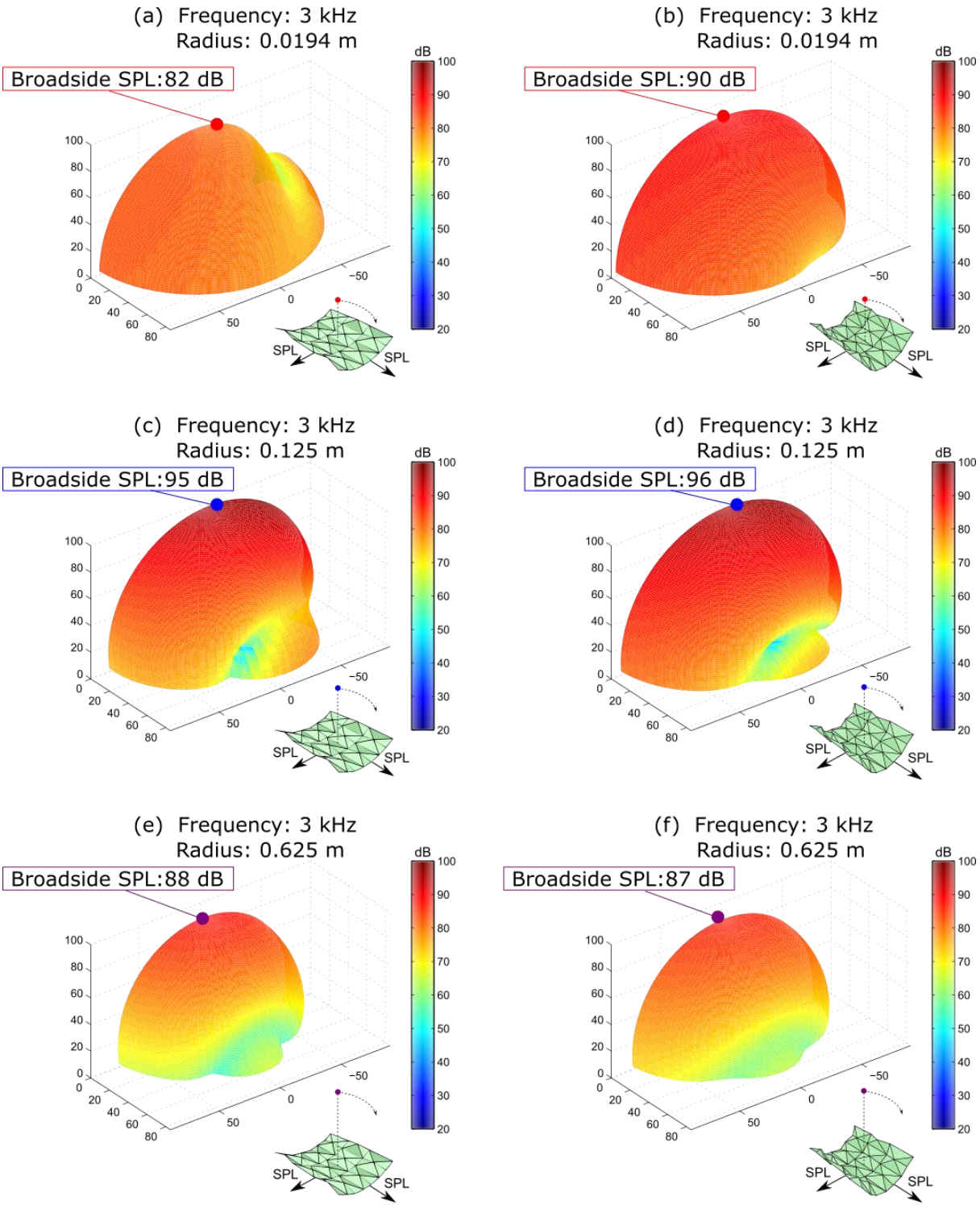

Figure 5: BEM results of two different folded configurations of the waterbomb array at a frequency of 3 kHz. The left column (a,c,e) displays a less folded configuration, while the right (b,d,f) is slightly more folded. The radial distance is (a,b) 0.0194 m, (c,d) 0.125 m, and (e,f) 0.625 m.

Figure 6 displays the BEM results for the same two folded configurations as in Figure 5, but at 9 kHz and at increasing radii of 0.0326 m, 0.125 m, and 0.625 m. This figure demonstrates the abilities of the

waterbomb array to guide acoustic energy. Between Figure 6(a) and Figure 6(c), broadside SPL increases by only around 1 dB; however, the number of lobes increases dramatically in Figure 6(c) as compared to Figure 6(a). One of these lobes, while not at broadside, has an amplitude of 94 dB, which is an increase of 5 dB from the maximum amplitude in Figure 6(a). The more folded configuration also sees focusing at this radial distance. As the radial distance is increased between Figure 6(b) and Figure 6(d), broadside SPL increases by 6 dB.

Folding also is shown to have an influence on the angular pattern of acoustic radiation. There is a reduction in SPL on Figure 6(b) that is not present in Figure 6(a). The surface plot in Figure 6(d) is at approximately uniform SPL, whereas Figure 6(c) shows more nodes than its more folded counterpart and a narrower beam at broadside.

Finally, folding is shown to have an influence on far field radiation. There is a significant reduction in broadside SPL in Figure 6(f) as compared to Figure 6(c): the less folded configuration has a far field broadside SPL of 94 dB while the more folded configuration has a far field broadside SPL of 81 dB, which is a significant reduction of 13 dB simply through folding. The general trend in the lobes and nodes in the far field is also of interest. Figure 6(e,f) demonstrate mostly uniform sound radiation in one direction, while displaying a number of nodes in the perpendicular direction.

The acoustic transducer array that is inspired by the waterbomb array displays several interesting acoustic features, including focusing both through folding and at different radial distances from the center of each array.

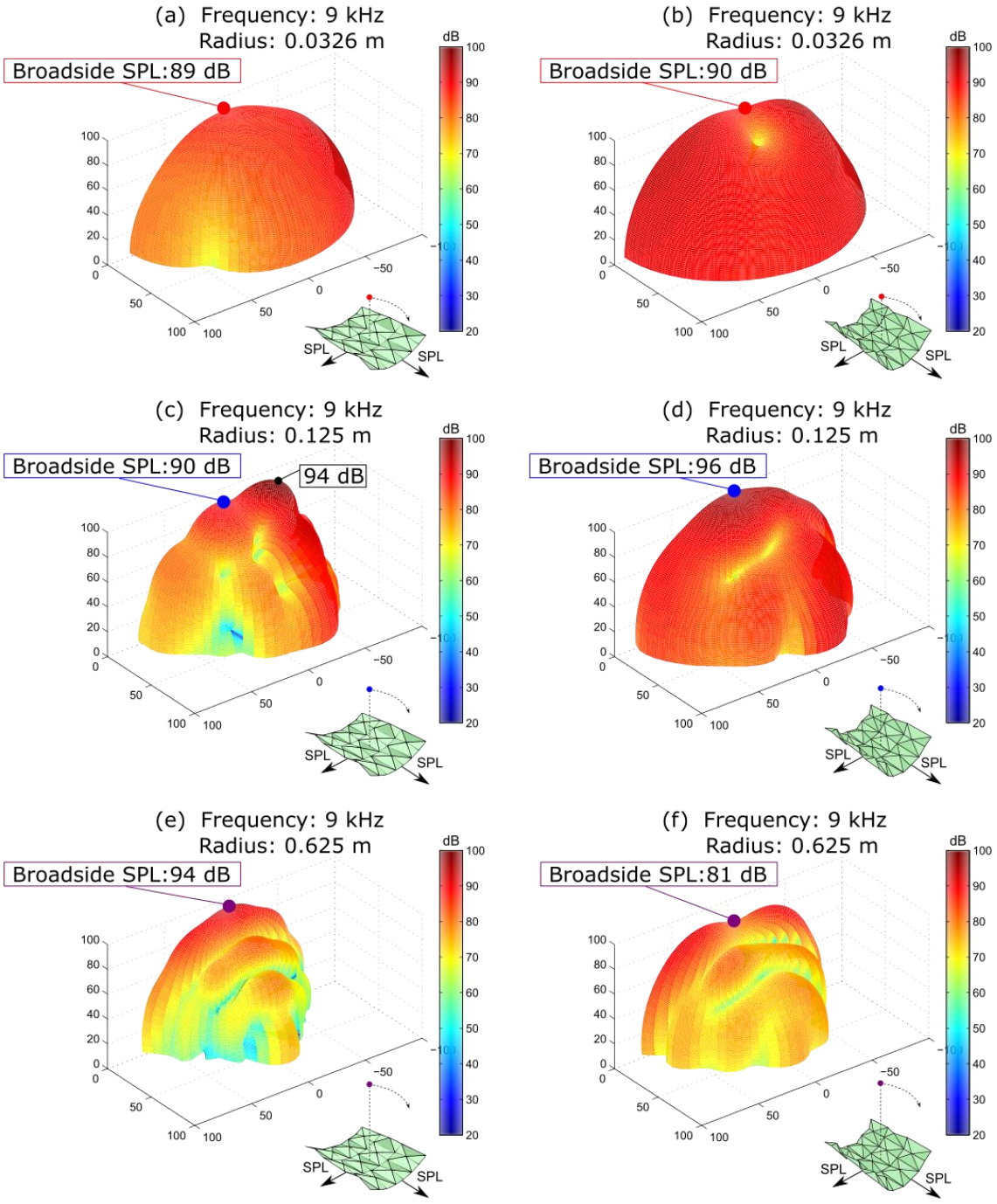

Figure 6: This figure displays the BEM results of two different folded configurations of the waterbomb array at a frequency of 9 kHz. The left column displays a less folded configuration (a,c,e), while the right (b,d,f) is slightly more folded. The radial distance is (a,b) 0.0326 m, (c,d) 0.125 m, and (e,f) 0.625 m.

3.2 Four-pointed star

Two folded configurations of the four-pointed star are examined through far field BEM computations at 13 kHz and at four azimuthal angles: φ=0, 22, 44.5, and 67˚. This folding pattern is made up of a triangular section that is repeated every 90˚, so these four azimuthal angles represent four "slices" of acoustic wave radiation between 0˚ and 90˚. These angles are represented in each of four quadrants of the polar plots that display predicted sound pressure level (SPL) in dB. The variable β indicates elevation angle, where β=0˚ occurs at broadside, perpendicular to the plane of the array. The SPL is evaluated in dB from the center of the polar plot. The insets in each of the plots demonstrate the extent of folding of the four-pointed star.

These figures demonstrate how folding can dramatically adjust the sound field produced by the array. In the φ=22˚ quadrant, the number of lobes decreases from three to two lobes as the array is folded from Figure 7(a) to Figure 7(b). Additionally, while one of the nodes is present at the same elevation angle for both folded configurations, at approximately β=30˚, the depth of the node is reduced in the more folded configuration. In the φ=0˚ quadrant, there are the same number of lobes for both configurations, but the second node migrates elevation angle; it moves from β=60˚ in Figure 7(a) and migrates to approximately β=55˚ in Figure 7(b). The φ=67˚ quadrant mirrors the red, φ=22˚ quadrant in the reduction in number and depth of nodes. The φ=44.5˚ quadrant demonstrates around a 3 dB reduction in SPL at the node position from Figure 7(a) to Figure 7(b). Additionally, the lobe at broadside is slightly wider in Figure 7(b) compared to Figure 7(a).

These results indicate that folding can greatly affect directivity. Simply adjusting the tessellation from a relatively unfolded state to a more folded state results in a decrease in nodes at each azimuth angle and a change in the width of some lobes.

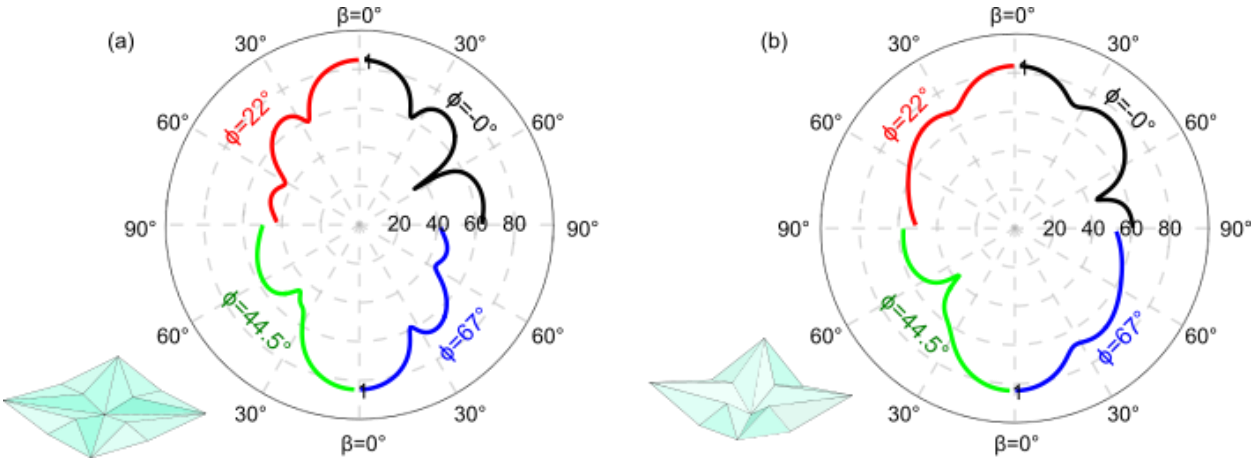

Figure 7: Far field BEM results for the four-pointed star at 13 kHz at two different folding angles. Four different azimuth angles are represented in each of four quadrants on each plot. The tessellated transducer geometry results as shown in part (a) are a less folded configuration of the transducer than for those results shown in (b). Each quadrant of the polar plot represents the simulations at one of four different azimuth angles, indicated by labels in each quadrant.

3.3 Comparison of six-pointed star and waterbomb unit cells

This section compares the BEM results of the waterbomb unit cell and a folding pattern called the six-pointed star. The six-pointed star unit cell is a variation on the four-pointed star unit cell generated in OMTO and described in detail in the last section. In addition to its similarities to the four-pointed star in Figure 4, this tessellation also bears similarities to the waterbomb unit cell from Figure 2(a). The tessellations are again compared in Figure 8 below. Both tessellations have alternating mountain and valley folds at the center, as indicated by the red and blue lines respectively, though the six-pointed star has 12 alternating folds, whereas the waterbomb unit cell has 8. The outer edge features signify another primary difference, as the outer red folds on the six-pointed star pattern change the features of the outer edges as compared to the waterbomb unit cell. These two patterns are both modeled in the BEM program to determine how two similarly sized unit cells produce different directivity results.

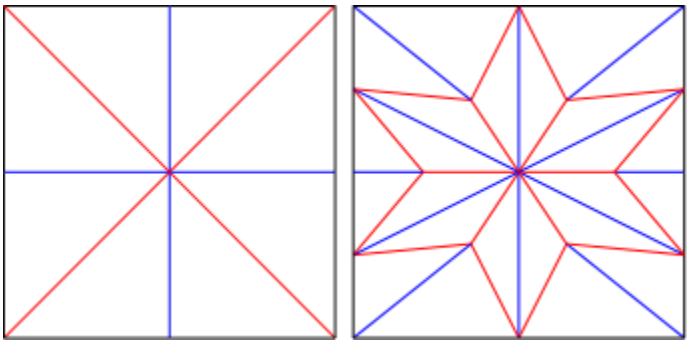

Figure 8: Waterbomb unit cell (left) and six-pointed star unit cell (right) both have alternating mountain and valley folds at the center, though their outer features are different.

The BEM results of these figures are shown below in Figure 9. Each subplot graphs SPL versus radial distance from the center of the array at broadside and at $\varphi=0^{\circ}$. The blue line corresponds to the unfolded configuration, the green to the slightly folded configuration, and the red to the most folded configuration; images of these configurations are present in insets beneath the respective plots. Each column corresponds to the results at 5 kHz, 10 kHz, and 20 kHz respectively.

For the lowest frequency of 5 kHz, the six-pointed star results show expected trends: SPL decreases as radial distance increases. The waterbomb results show more significant differentiation between the different folding arrangements than do the six-pointed star results. The six-pointed star results line up very closely regardless of folding arrangement. It can be observed that folding does not introduce significant differences in SPL amplitude at any radius for the 5 kHz frequency. At the 10 kHz frequency, there is greater differentiation in radiated SPL between the three folding arrangements, particularly as the radial measurement increases. At about a radius of 0.03 m, all folding configurations have approximately the same SPL. Yet, at the 0.47 m radius, there is around a 5 dB difference in SPL between the least folded and most folded configurations. So at 10 kHz, there is greater differentiation between folded configurations at greater radial measurements. At 20 kHz, some focusing can be observed. The unfolded configuration has an SPL of 100 dB at 0.01 m which increases significantly to 108 dB at 0.03 m. The slightly and more folded configurations also demonstrate a small increase in SPL as radius increases between 0.01m and 0.03 m,

though it is not as dramatic as the 8 dB difference observed in the unfolded configuration. At low frequencies, the six-pointed star tessellation does not demonstrate significant focusing or change in amplitude through folding. The higher, 20 kHz frequency plots do demonstrate focusing by the unfolded array and slight focusing at the more folded configurations.

Compared to the results of the six-pointed star tessellated array, the waterbomb tessellated array yielded more differentiated results. At the 5 kHz frequency, the results of all three folding configurations show the expected trend of decreasing SPL with increasing radial distance. On the other hand, the results for the most folded configuration have significantly higher SPL than the unfolded configuration: there is around a 6 dB difference between the unfolded and most folded SPLs at the lowest radial distance of measurement. This trend does show an opportunity for focusing through folding, as at all radial measurements the most folded SPL results are greater than the slightly folded SPL results, and the slightly folded SPL results are greater than the unfolded SPL results.

At the 10 kHz frequency for the waterbomb tessellation, all three of the folding configurations demonstrate focusing. The unfolded and slightly folded configurations peak at about 0.06 m, while the most folded configuration peaks around 0.03 m. Additionally, while in the 5 kHz plot the most folded configuration saw the highest SPL, here the unfolded configuration has the highest SPL.

At the 20 kHz frequency, there are again signs of focusing. Both the unfolded and most folded plots increase in amplitude by about 10 dB as the radius increases from 0.01 m to 0.03 m. The slightly folded configuration shows a reversing trend, starting with high 100 dB SPL, reducing to 88 dB around 0.06 m, and increasing again from there. Each of these changes in SPL through increase in radius show opportunity for focusing using this array. Additionally, the slightly folded configuration has a high, 100 dB amplitude at 0.01 m, which is 8 dB above the unfolded configuration and 15 dB above the most folded configuration at that same radius. This shows an excellent opportunity for focusing through folding.

The similarly-sized waterbomb and six-pointed star tessellations yield very different results with respect to changes in SPL as radial distance increases. The six-pointed star tessellation yielded mostly uniform result, with the possibility of focusing through folding at some higher frequencies. On the other hand, all three frequencies that the waterbomb tessellation were examined at yielded interesting results. At the lower, 5 kHz frequency, there is clear potential for focusing through folding, while at the higher frequencies focusing may be achieved either through folding or through changes in radial measurement. The waterbomb array yielded very useful and interesting results that may be examined further in the future.

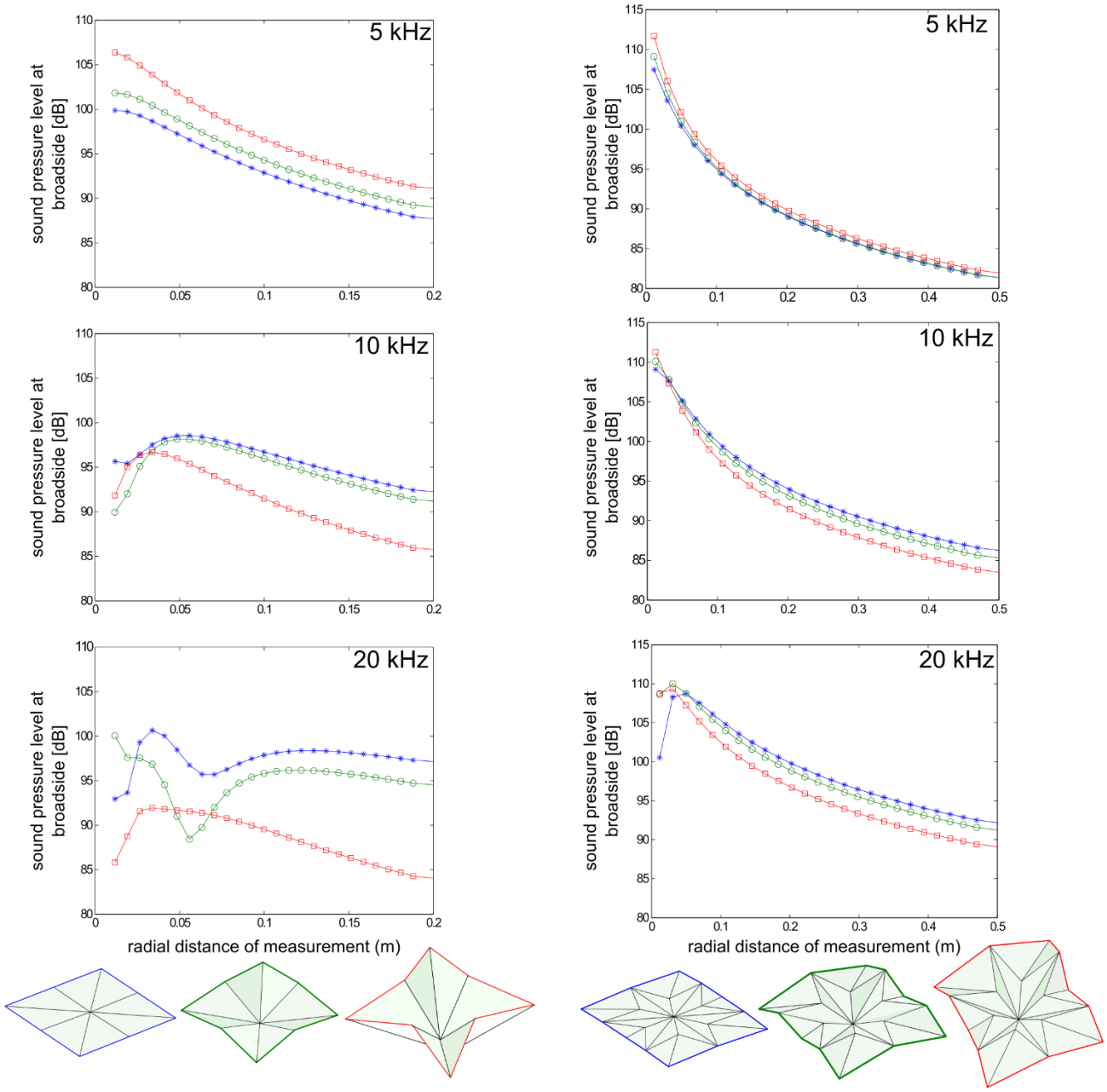

Figure 9: Each of the plots in this figure plots SPL at broadside [dB] versus the radial distance of measurement [m] from the center of the respective array. The first column of graphs are the results for the waterbomb unit cell at 5 kHz, 10 kHz, and 20 kHz. Each plot displays the results for three configurations of the unit cell, as represented by the folded models beneath the plots. The blue lines represent the unfolded configuration, the green a slightly folded configuration, and the red a more folded configuration. The second column of graphs are the results for the six-pointed star tessellation at 5 kHz, 10 kHz, and 20 kHz.

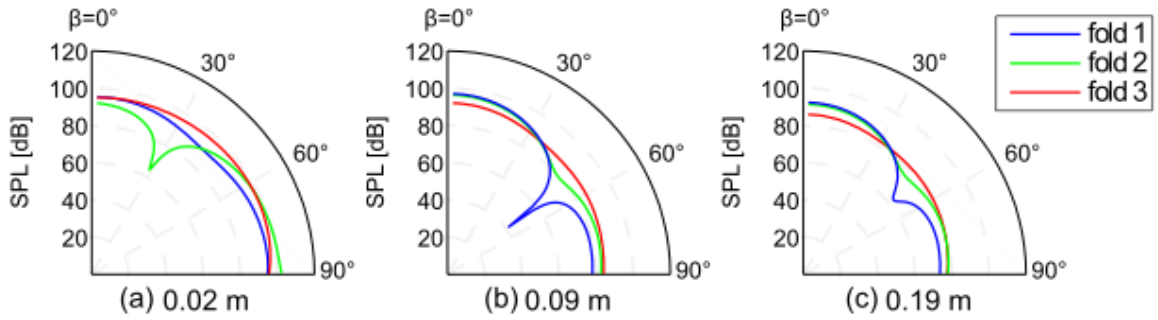

Figure 10: SPL [dB] over all elevation angles for the waterbomb unit cell at 10 kHz and at an azimuth of ~0 deg. The blue line represents the unfolded configuration, the green represents the slightly folded configuration, and the red the most folded configuration, as defined in Figure 9. Each inset represents the SPL at the labeled distances from the center of the array.

Figure 10 shows the SPL over all elevation angles at an azimuth angle of 0 deg at 10 kHz. Each inset gives the SPL at three different radial distances of measurement from the center of the array. The most folded configuration does not show much variation between radii, remaining mostly uniform between Figure 10(a), Figure 10(b), and Figure 10(c). The slightly folded configuration displays a ~10 dB reduction around β=30˚ in Figure 10(a). Yet, at the higher radial distances of measure in Figure 10(b,c), the SPL is mostly uniform. This data does show an opportunity for focusing through folding, as the second folded configuration does have a higher broadside SPL than the other two folds in Figure 10(a). The least folded configuration has a node in Figure 10(b) and Figure 10(c) at around 65 ˚, though there is around 20dB difference in depth between Figure 10(b) and Figure 10(c).

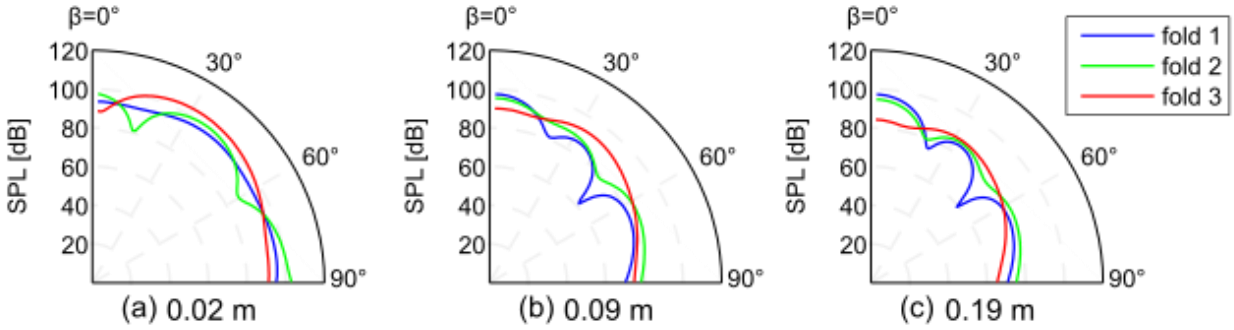

Figure 11: SPL [dB] over all elevation angles for the waterbomb unit cell at 20 kHz and at an azimuth of ~0 deg. The blue line represents the unfolded configuration, the green represents the slightly folded configuration, and the red the most folded configuration, as defined in Figure 9. Each inset represents the SPL at the labeled distances from the center of the array.

The most folded configuration, fold 3, shows a lower SPL at broadside than SPLs associated with the other two configurations at all three of the radial distances of measurement. Each of these configurations sees an increase in amplitude around β=3˚, indicating how elevation angle has an effect on folding. The unfolded

configuration is mostly uniform at the lowest radial distance in Figure 11(a), though it shows the evolution of lobes and nodes at the higher radial distances in Figure 11(b,c). The positions of lobes and nodes of the slightly folded configuration shift positions as radius increases, indicating how the entire pattern of directivity is affected by changing the radius, instead of simply a change in amplitudes. These results emphasize how simple changes in folding arrangement and radial distance for the waterbomb array may have an impact on radiated SPL and the pattern of acoustic wave radiation in space

3.4 Planar and line arrays of the six-pointed star and waterbomb constituents

Mailloux [26] discusses the characteristics of linear and planar arrays at length. Linear arrays create a pattern of acoustic wave radiation in space called a fan beam, where the beam fans out along the same axis as the array but remains narrow in the perpendicular axis. Postema [5] recognizes that one-dimensional linear and curved arrays are commonly used for diagnostic ultrasound arrays. Curvilinear arrays result in a sound field that diffuses outwardly. Figure 12 depicts a curvilinear array made up of the six-pointed star constituent. As the tessellation folds, it forms a shape that would emit sound diffusely.

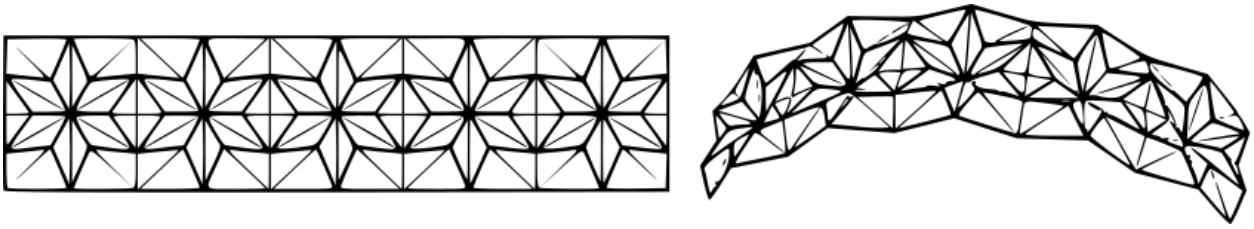

Figure 12: Unfolded and folded configurations of a 1x5 linear array of the six-pointed star constituent.

Likewise, two-dimensional arrays provide a unique opportunity for sound focusing in ultrasonics. Rows and columns in a two-dimensional array may be independently phased to assist in sound focusing [5]. Planar, two-dimensional acoustic arrays show increased directivity as compared with a single constituent [26] and, in the case of arrays that are symmetric in both axes, will extend the pattern of a linear strip of the array in the direction perpendicular with it [27].

Based on the results of the previous sections of this thesis, it is a useful next step to investigate the folding configurations of two-dimensional arrays so as to assess opportunities for focusing by virtue of the folding operations.

Figure 13 depicts a 4x4 six-pointed star array that was input into ROS, along with two of the folded configurations. The folding shapes of this tessellation begin as a cylindrically shaped fold in the vertical axis before the tessellation naturally locks and begins cylindrically folding along the horizontal axis. This adaptation provides interesting opportunity for sound focusing. Curved, satellite-shaped surfaces are effective at focusing waves. A folding pattern like the one depicted in Figure 13 with piezoelectric materials bonded to the surfaces pictured would result in a diffuse sound field for the middle image and a more focused sound field for the image on the right. The sound field could be adapted from diffuse to focused through simple folding.

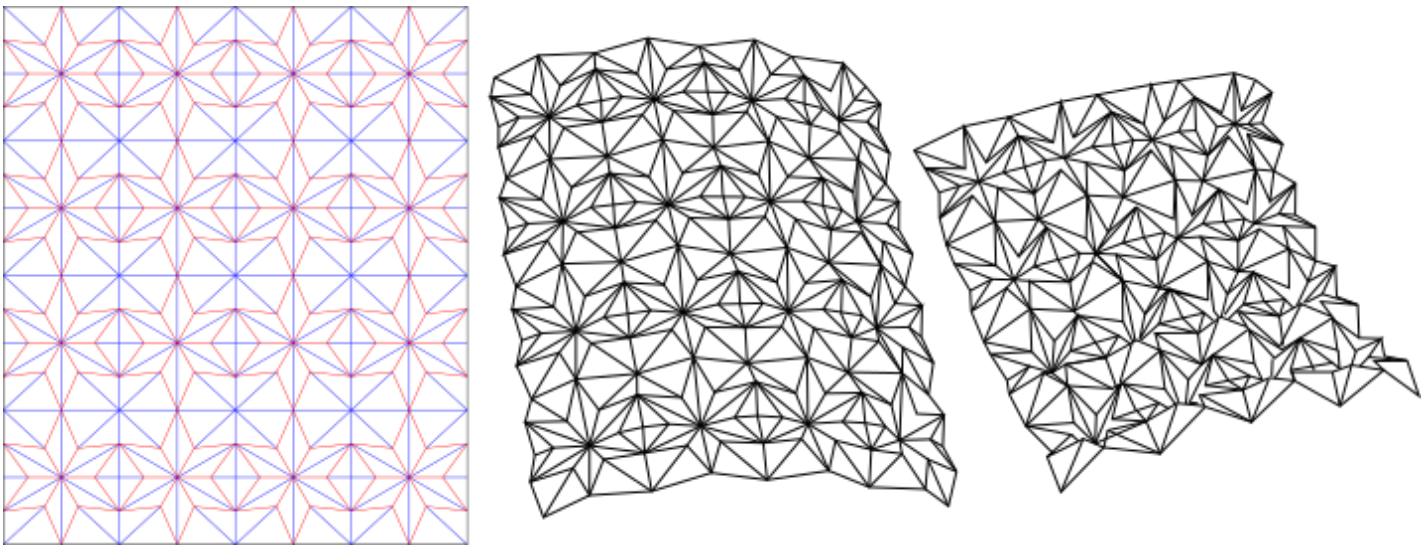

Figure 13: The six-pointed star creates a cylindrical fold along one axis before locking and beginning to fold along a perpendicular axis. On the left is the folding pattern created in Inkscape and input into ROS. The other two images are configurations of the origami fold taken from ROS.

A 4x4 waterbomb array was also created in Inkscape and folded in ROS and the results are depicted in Figure 14. This array creates a simple, cylindrical shape through folding. This cylindrical shape does provide opportunity through focusing at the array's focal point which will change position based on the degree of folding of the array. On the other hand, these arrays that fold cylindrically provide usable sound radiation only insofar as they do not fold over onto themselves.

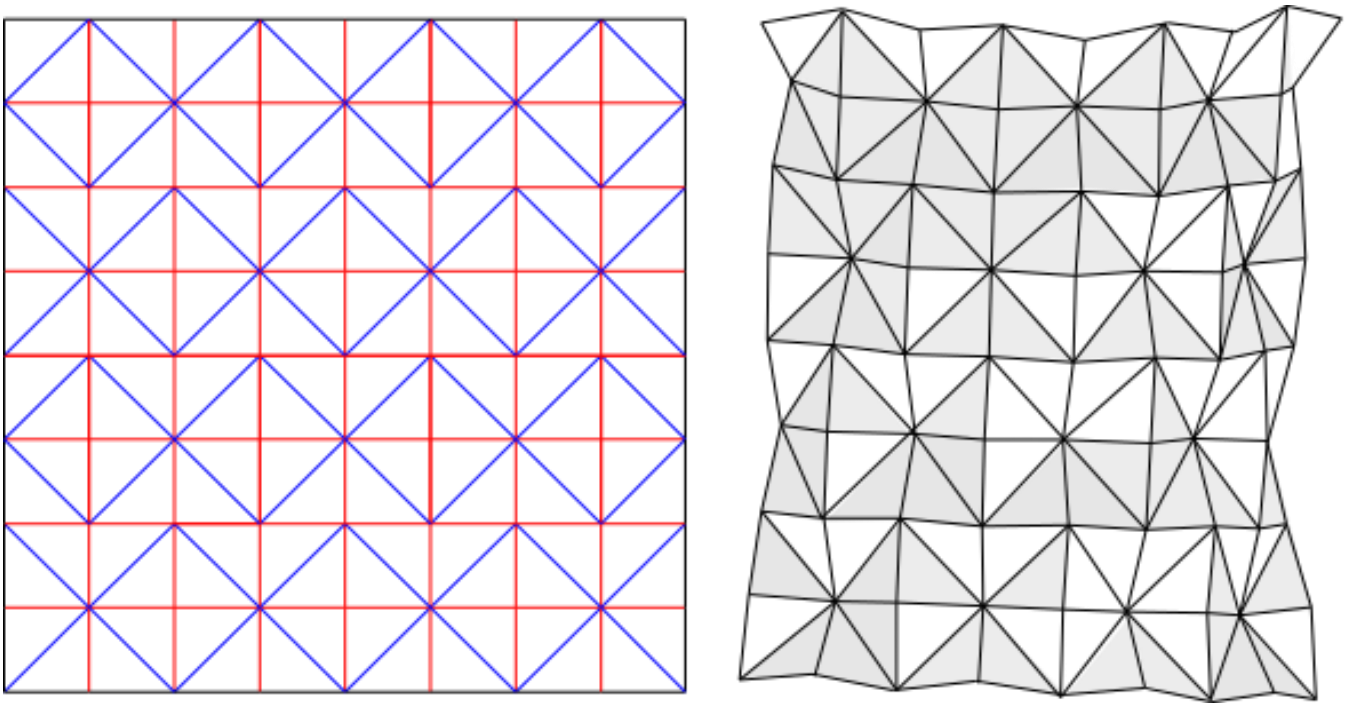

Figure 14: The 4x4 waterbomb array folds cylindrically about the vertical axis. The two images represent an unfolded and slightly folded state of this array produced by ROS.

Acoustic beamformers that consist only of a single constituent or unit cell are limited in their abilities to focus or direct sound. Arrays of constituents like the six-pointed star and the waterbomb unit cell result in more interesting acoustic results than a single constituent alone. Arrays as large as these cannot be efficiently run in the existing BEM code; however, the interesting trends observed for the constituents make a compelling argument for them to be analyzed further.

4 Conclusions

The ability to direct and focus acoustic energy is utilized in a number of technologies. These technologies use acoustic transducer arrays that guide acoustic energy through artificially introduced constructive and destructive interference that result in the radiation of the desired sound field. These technologies are computationally complex to design and are limited in their portability, so a new design—a foldable, origami-inspired acoustic transducer array—is proposed to bypass these challenges.

Miura-ori has been studied in the past as a potential tessellation on which to model one of these transducer arrays, but it is far from the only folding pattern that yields interesting acoustic results. This research aims to characterize the influences that different tessellations and folding arrangements have on these transducer arrays, and begins this by creating a streamlined, iterative design process which aids in the design and evaluation of new tessellations. These research focused on the study of four tessellations.

The first step in this process is to choose a new design, which is done either by taking inspiration from literature or by using an origami topology optimizer like OMTO. These designs are then folded in the Rigid Origami Simulator, which produces images of the way that the origami tessellation folds. Here, the user visually inspects the folding arrangements to determine if the folding pattern displays useful characteristics, including dynamic shape change through folding, flat-foldability, or curved folding shapes.

The folding pattern then can be evaluated in a BEM code which simulates the radiated SPL from the center of the array. The tessellations examined in this research have results that show promise for the use of origami-inspired acoustic transducer arrays to direct and focus sound energy. The process outlined by this research allows for new tessellations to be generated and tested quickly and easily. The 4x4 waterbomb array provides opportunities for focusing through simple folding motions, as well as focusing at different distances of measure from the center of the array. Even at the low, largely uniform frequency of 3 kHz, trends can be observed in the location and depth of lobes and nodes that suggest this tessellation has promise. At the 9 kHz frequency, clear amplification of sound can be observed simply through folding. The four-pointed star unit cell, likewise, shows the effect that folding has on the radiation of acoustic waves from the array. The position and width of the lobes and the depth of the nodes changes as the degree of folding changes for the same azimuth angle. Additionally, changes in azimuth angle also result in marked differences in SPL at all elevation angles, suggesting that orientation matters in the use of a tessellation like this one.

The single waterbomb constituent shows very dynamic changes in broadside SPL through folding that offer opportunities for focusing. Arrays of these constituents create curved folding shapes, which also provide opportunities for folding. The similar six-pointed star constituent does not show the same opportunities for focusing, though arrays of these constituents result in interesting folding behavior that suggest opportunities for creating focused and diffused sound fields with the array.

Future efforts towards making this process more efficient might examine the development of an analytical code like the one developed for Miura-ori in previous research [15]. The existing BEM code does not

deliver very efficient results, particularly larger arrays like those in this work. As it stands, the tessellation must have mathematically definable geometric relationships, which can be difficult to determine. Yet, as the analytical code is orders of magnitude more time efficient than the BEM code for Miura-ori in this prior work, a more time-efficient evaluation may prove useful in the future. Additional endeavors may be made toward experimentally verifying key results from BEM simulations, as Harne and Lynd [11] have previously done. Streamlining the process of making and testing a physical specimen are also necessary explorations in the future.

The results documented in this and previous research done by this team, show the potential of origami-inspired acoustic beamformers. Basic, folding-induced shape changes can have an enormous effect on the way that an origami-inspired array or constituent radiates sound. These arrays have the ability both to steer and focus sound, simply through changing the way a specimen is folded. The process detailed in this research will help streamline the process of developing new arrays and further investigations into this very promising field of acoustic beamfolding.

References

[1] B. Harker, K. Gee, T. Neilsen, A. Wall and M. James, "Phased-array measurements of full-scale military jet noise," *Proceedings of the 20th AIAA/CEAS Aeroacoustics Conference*, pp. 2014-3069, 2014.

[2] D. Simons, M. Snellen, B. van Midden, M. Arntzen and D. Bergmans, "Assessment of noise level variations of aircraft flyovers using acoustic arrays," *Journal of Aircraft*, vol. 52, pp. 1625-1633, 2015.

[3] J. Panda, R. Mosher and B. Porter, "Noise source identification during rocket engine test firings and a rocket launch," *Journal of Spacecraft and Rockets*, vol. 51, pp. 1761-1772, 2014.

[4] M. Fink, G. Montaldo and M. Tanter, "Time-reversal acoustics in biomedical engineering," *Annual Reviews of Biomedical Engineering*, pp. 5: 465-497, 2003.

[5] M. Postema, Fundamentals of Medical Ultrasonics, New York: Spon Press, 2011.

[6] W. Eisenmenger, "The mechanisms of stone fragmentation in ESWL," *Ultrasound in Medicine and Biology*, vol. 27, no. 5, pp. 683-693, 2001.

[7] C. Coussios, C. Farny, G. ter Haar and R. Roy, "Role of acoustic cavitation in the delivery and monitoring of cancer treatment by high-intensity focused ultrasound (HIFU)," *International Journal of Hyperthermia*, vol. 23, no. 2, pp. 105-120, 2007.

[8] M. Shin, S. Lee, F. Fazi, P. Nelson, D. Kim, S. Wang, K. Park and J. Seo, "Maximization of acoustic energy difference between two spaces," *The Journal of the Acoustical Society of America*, vol. 128, no. 1, pp. 121-131, 2010.

[9] *Product Sheet: LRAD 100X*, San Diego, CA: LRAD Corporation, 2015.

[10] J. Jensen, S. Nikolov, K. Gammelmark and M. Pedersen, "Synthetic aperature ultrasound imaging," *Ultrasonics*, vol. 44, pp. e5-e15, 2006.

[11] R. Harne and D. Lynd, "Origami acoustics: using principles of folding structural acoustics for simple and large focusing of sound energy," *Smart Materials and Structures*, vol. 25, no. 8, 2016.

[12] A. Evans, J. Silverberg and C. Santangelo, "Lattice Mechanics of Origami Tessellations," *Physical Review E*, vol. 92, no. 1, 2015.

[13] J. Silverberg, A. Evans, L. McLeod, R. Hayward, T. Hull, C. Santangelo and e. al, "Using origami design principles to fold reprogrammable mechanical metamaterials," *Science,* vol. 345, pp. 647-650, 2014.

[14] T. Evans, "Deployable and Foldable Arrays of Spatial Mechanisms," *All Theses and Dissertations,* vol. Paper 5321, 2015.

[15] D. Lynd and R. Harne, "Strategies to predict time-harmonic radiated sound fields from fodlable, tessellated, Miura-ori-based transducer arrays for acoustic beamfolding," 2016.

[16] M. Schenk and S. Guest, "Geometry of Miura-folded metamaterials," *Proceedings of the National Academy of Sciences,* vol. 110, pp. 3276-3281, 2013.

[17] P. Sareh and S. Guest, "Design of non-isomorphic symmetric descendants of the Miura-ori," *Smart Materials and Structures*, vol. 24, no. 8, 2015.

[18] P. Sareh and S. Guest, "Design of isomorphic symmetric descendants of the Miura-ori," *Smart Materials and Structures*, vol. 24, 2015.

[19] M. Bendsoe and N. Kikuchi, "Generating optimal topologies in structural design using a homogenization method," *Computer Methods in Applied Mechanics and Engineering,* vol. 71, pp. 197-224, 1988.

[20] R. Lang, "Origami: Complexity in Creases (Again)," *Engineering and Science,* vol. 67, no. 1, pp. 5-19, 2004.

[21] Cromwik, "Numerical folding of airbags based on optimization and origami," Chalmers University of Technology, 2007.

[22] K. Fuchi, P. Buskohl, G. Bazzan, M. Durstock, G. Reich, R. Vaia and J. Joo, "Origami Actuator Design and Networking Through Crease Topology Optimization," *Journal of Mechanical Design,* vol. 137, 2015.

[23] T. Tachi, "Rigid Origami Simulator," [Online]. Available: www.tsg.ne.jp/TT/software/.

[24] T. Tachi, "Simulation of rigid origami," in *Origami 4*, 2009, pp. 175-187.

[25] F. Holmstrom, "Structure-acoustic analysis using BEM/FEM; Implementation in Matlab," Lund University, Lund, 2001.

[26] R. Mailloux, Phased array antenna handbook, Boston: Artech House, 2005.

[27] A. Berkhout, D. de Vries and P. Vogel, "Acoustic control by wave field synthesis," *Journal of the Acoustical Society of America,* vol. 93, no. 5, pp. 2764-2778, 1993.

[28] K. Fuchi and A. Diaz, "Origami Design by Topology Optimization," *Journal of Mechanical Design*, vol. 135, no. 11, 2013.